An approximation of the inverse Ricker wavelet as an initial guess for bidirectional deconvolution

Qiang Fu, Yi Shen and Jon Claerbout

ABSTRACT

Bidirectional deconvolution is a powerful tool for performing blind deconvolution on a signal that contains a mixed-phase wavelet, such as seismic data. Previously, we used a prediction error filter (PEF) as the minimum-phase filter and an impulse function as the maximum-phase filter as initial guesses. This surprised us by apparent instability as the solution would jump from spiking the first pulse of a Ricker wavelet to get larger middle pulse. In this paper, we propose new initial guesses for the causal and anti-causal deconvolution filters that are more effective on data with a Ricker-like wavelet. We test these on both synthetic data and field data. The results demonstrate that the new starting filters do a better job than the previous initial guesses.

INTRODUCTION

Zhang and Claerbout (2010) proposed a new method for blind deconvolution to overcome the minimum-phase assumption, called "bidirectional deconvolution". A seismic data trace can be represented by a convolution of a wavelet with a reflectivity series,

$$d = r * w, \tag{1}$$

where d denotes the seismic data trace, r denotes the reflectivity series, and w denotes a wavelet.

In conventional blind deconvolution, we assume that w is a minimum-phase wavelet. However this assumption is not applicable for field seismic data. If w denotes a mixed-phase wavelet, it can be represented by a convolution of two parts: $w = w_a * w_b^r$, where w_a is a minimum-phase wavelet and w_b is a reversed minimum-phase wavelet; hence w_b^r itself is a maximum-phase wavelet. (The superscript r denotes reversed in time.) Thus equation 1 can be rewritten as

$$d = r * (w_a * w_b^r). \tag{2}$$

If we know the inverse filters f_a and f_b^r for w_a and w_b^r, respectively, to satisfy

$$\begin{cases} w_a * f_a = \delta(n) \\ w_b * f_b = \delta(n) \end{cases}, \tag{3}$$

we can recover the reflectivity series:

$$r = d * f_a * f_b^r, \tag{4}$$

where filter f_a is the inverse signal of w_a and filter f_b is the inverse signal of w_b

Now we can use nonlinear inversion to solve this blind deconvolution problem for a mixed-phase wavelet by solving the two equations below alternately:

$$\begin{cases} (d * f_b^r) * f_a = r_a \\ (d * f_a)^r * f_b = r_b^r \end{cases} \tag{5}$$

where both f_a and f_b are minimum-phase signals.

Shen et al. (2011) proposed another method to solve equation 4. Instead of solving for f_a and f_b alternately, they solve f_a and f_b simultaneously. Using this new approach allows us to estimate results with similar waveforms for f_a and f_b, which is a natural characteristic for data with a Ricker-like wavelet. In addition, this new method is faster than previous one. Hence we will use this to perform bidirectional deconvolution.

Since bidirectional deconvolution is a nonlinear problem, it requires that the starting model be close to the true one, and it is highly sensitive to the initial guess for both f_a and f_b. Shen et al. (2011) uses a simple one-spike impulse function for both filters. However, sometimes the true model does not resemble an impulse function. Therefore, we attempt to find a better initial guess.

APPROXIMATION OF THE INVERSE RICKER WAVELET

Generally, it is a complicated issue to find a good initial guess for bidirectional deconvolution. However, in most field and synthetic geophysical data the wavelet is similar to a Ricker wavelet. For example, band-limited marine seismic data with ghosts and the land response of an accelerometer are both Ricker-like. Hence Ricker-like wavelets have broad applicability. For this reason, we choose a Ricker wavelet to approximate the wavelet of the data and derive the initial filters from the inverse Ricker wavelet. If we could derive the inverse of the Ricker wavelet, it would provide a suitable initial guess.

In theory, however, Ricker wavelets do not have a stable inverse. Therefore we must find an approximate inverse to use as the initial guesses for filters f_a and f_b. Since we need two initial guesses, one for each filter, our approximate inverse should consist of two symmetric parts.

We have three tasks: first we must find a finite approximation for the continuous Ricker wavelet; second we must separate the approximate form into two symmetric parts; and third we must find a way to avoid the singularity problems we encounter

when inverting these two parts directly in the frequency domain. Let's address these tasks one by one.

Finite approximation

It is known that a Ricker wavelet is the second-order derivative of a Gaussian function. For computation, we use a finite and discrete approximation to a Ricker wavelet as a replacement to the infinite and continuous real second-order derivative of a Gaussian function. We use a second-order finite-difference operator to approximate a second-order derivative and binomial coefficients to approximate a Gaussian function.

In the Z domain,

$$\text{Ricker} = -(1-Z)^2(1+Z)^{2N}. \tag{6}$$

The parameter N is half the order of the binomial we used. Here we use $2N$ in equation 6 instead of N simply to keep the order of the binomial even to facilitate the later separation. In practice, we would choose the value of N parameter according to the wavelength (or principle frequency component) of the wavelet in our data. The larger the value, the wider the wavelet.

Figures 1(a) and 1(b) show this fourth-order (N=4) finite approximation of the Ricker wavelet in the time and frequency domains. Here we use the fourth-order as an example, but we can use a different-order implementation as long as the approximate Ricker wavelet has the same wavelength (or principle frequency component) as the wavelet of our data.

Separation

We can manipulate equation 6 and decompose it into two symmetric parts. First, we shift the Ricker wavelet to the center of the axes:

$$\text{Ricker} = -\frac{(1-Z)^2}{Z}\frac{(1+Z)^{2N}}{Z^N} \tag{7}$$

which rearranges to

$$\text{Ricker} = [(1-\frac{1}{Z})(1+\frac{1}{Z})^N][(1-Z)(1+Z)^N]. \tag{8}$$

We call one of these symmetric parts a "half-Ricker wavelet":

$$H(Z) = (1-Z)(1+Z)^N \tag{9}$$

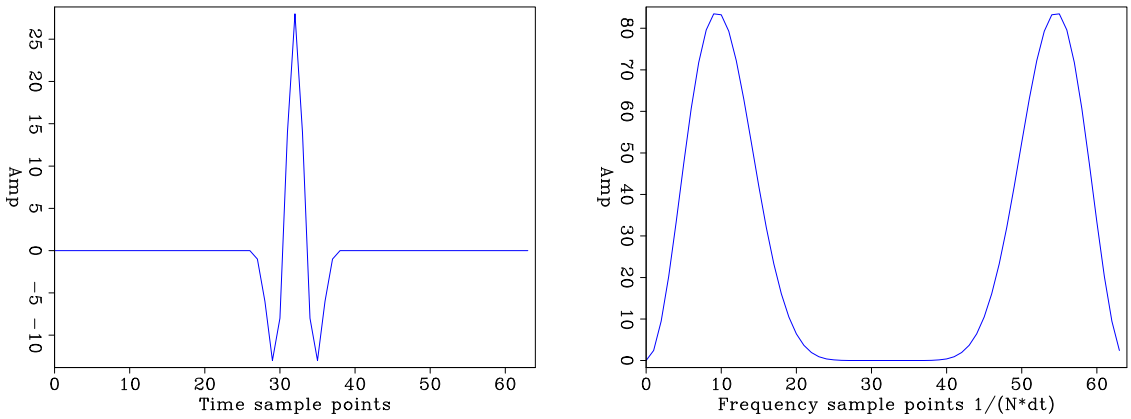

(a) (b)

Figure 1: The fourth-order finite approximation of the Ricker wavelet: (a) in the time domain; (b) in the frequency domain. [**ER**]

Figures 2(a) and 2(b) show this finite approximation of the Ricker wavelet in the time and frequency domains.

We denote the inverse of the half-Ricker wavelet, which is our candidate as the initial guess for both filter f_a and filter f_b^r, as $\hat{f}_a$ and $\hat{f}_b^r$ in the time domain and $\hat{F}_a$ and $\hat{F}_b^r$ in the Z domain:

$$\begin{cases} \hat{F}_a(Z) = \hat{F}_b(Z) = \frac{1}{H(Z)} = \frac{1}{(1-Z)(1+Z)^N} \\ \overline{\hat{F}_b^r(Z)} = \hat{F}_b^r(\frac{1}{Z}) = \frac{1}{H(\frac{1}{Z})} = \frac{1}{(1-\frac{1}{Z})(1+\frac{1}{Z})^N} \end{cases} \tag{10}$$

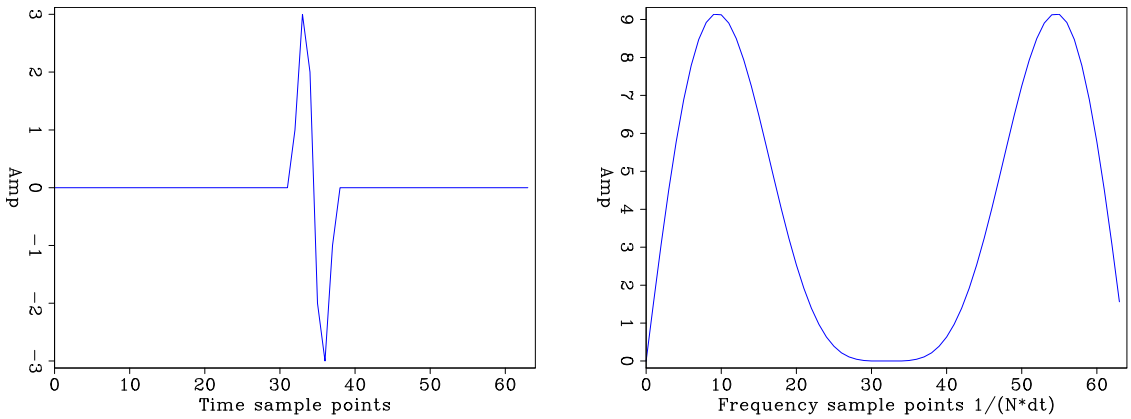

(a) (b)

Figure 2: The fourth-order half-Ricker wavelet: (a) in the time domain; (b) in the frequency domain. [**ER**]

Avoiding the singularity

In the Z domain, the half-Ricker wavelet has two zeros, which makes it impossible to directly invert. Therefore, we modify the formula with two new factors to avoid errors caused by dividing by zero:

$$\hat{F}_a(Z) = \hat{F}_b^r(Z) = \frac{1}{H(Z)} = \frac{1}{(1-\rho_1 Z)(1+\rho_2 Z)^N} \tag{11}$$

For simplicity, we use the same value for ρ_1 and ρ_2, $\rho = \rho_1 = \rho_2$.

Figures 3(a) and 3(b) show the fourth-order Ricker wavelet in the time and frequency domains with different ρ values.

Figures 4(a) and 4(b) show the fourth-order half-Ricker wavelet in the time and frequency domains with different ρ values.

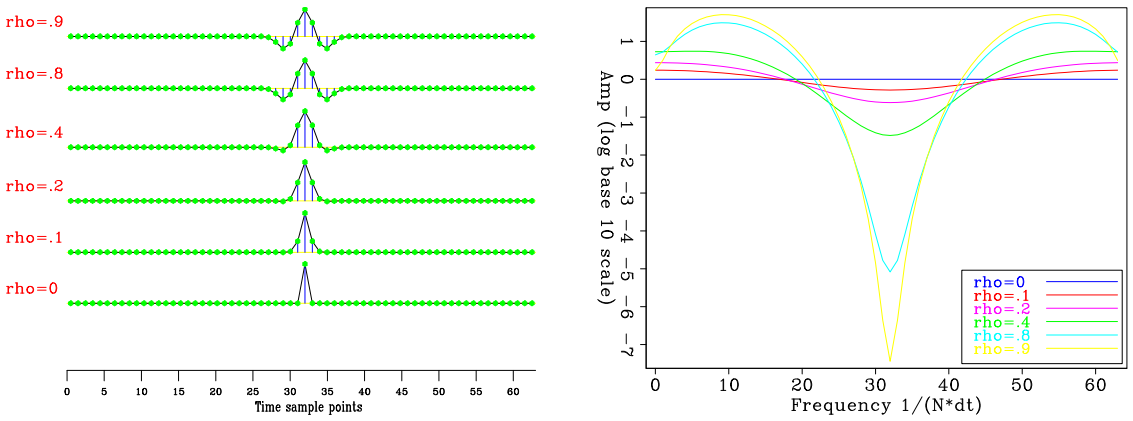

(a) (b)

Figure 3: The fourth-order Ricker wavelet with different ρ values: (a) in the time domain; (b) in the frequency domain. [**ER**]

Since we have $\hat{f}_a$ and $\hat{f}_b^r$ in the Z domain ($\hat{F}_a$ and $\hat{F}_b$), we have two methods to recover time-domain filter coefficients. The first one is to use $Z = e^{iw}$ to get frequency domain filters and then transfer them into the time domain by an inverse Fourier transform. Another method is to use a Taylor expansion to get time-domain filter coefficients. In theory, the two methods should be the same. For less accuracy problem, we always use the frequency method in this paper.

Finally we obtain the approximate inverse Ricker wavelet. Figures 5(a) and 5(b) show the inverse fourth-order causal half-Ricker wavelet ($\hat{f}_a$) in the time and frequency domains with different ρ values. The inverse anti-causal half-Ricker wavelet ($\hat{f}_a^r$) can be generated by reversing $\hat{f}_a$ along the time axis. $\hat{f}_a$ and $\hat{f}_a^r$ will be our initial guesses for bidirectional deconvolution.

To test how good our approximation of the inverse Ricker wavelet is, we convolve our fourth-order approximate Ricker wavelet (with no ρ factor) with our inverse Ricker

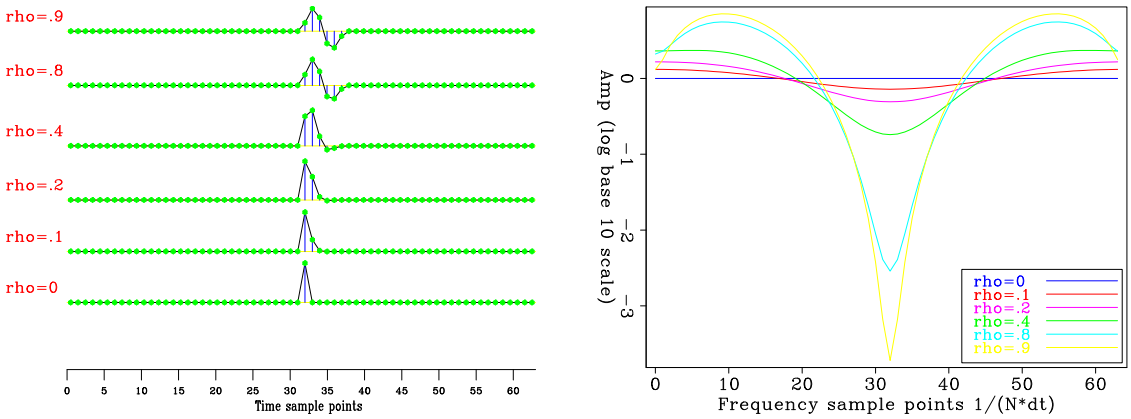

(a) (b)

Figure 4: The fourth-order half-Ricker wavelet with different ρ values: (a) in the time domain; (b) in the frequency domain. [**ER**]

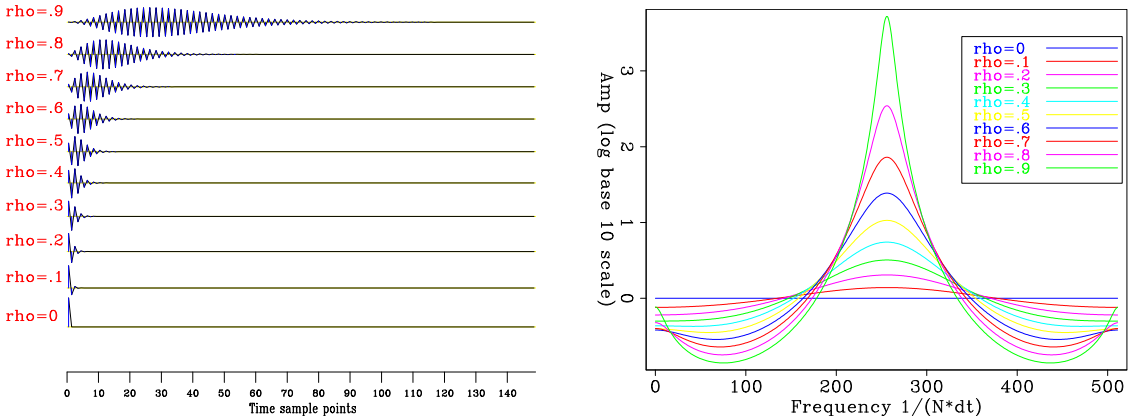

(a) (b)

Figure 5: The inverse fourth-order causal half-Ricker wavelet ($\hat{f}_a$) with different ρ values: (a) in the time domains ; (b) in the frequency domain. [**ER**]

wavelet (equation 12).

$$\text{test result} = \text{Ricker} * \hat{f}_a * \hat{f}_b^r \tag{12}$$

If our inversion is good, the output should be a spike in the time domain and a flat spectrum in the frequency domain.

Figures 6(a) and 6(b) show the test result in the time domain and the frequency domain with different ρ values. We see for $\rho = .9$ we get a good result. In particular, the frequency spectra are flatten as ρ increases.

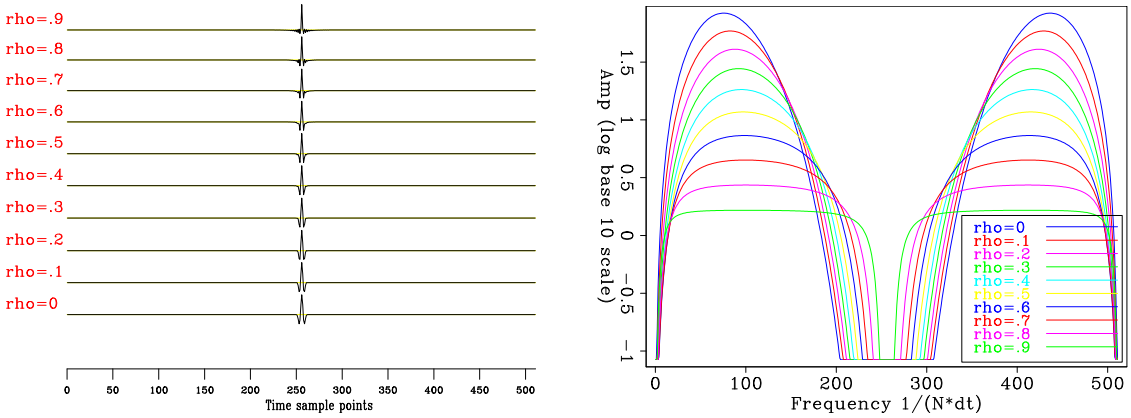

(a) (b)

Figure 6: The test results with different ρ values: (a) in the time domain; (b) in the frequency domain. [**ER**]

Large ρ value can yield even better results. For large ρ, the frequency spectra are almost flat, except for two zero-value points (at 0 frequency and the Nyquist frequency). Figures 7(a) and 7(b) show these results.

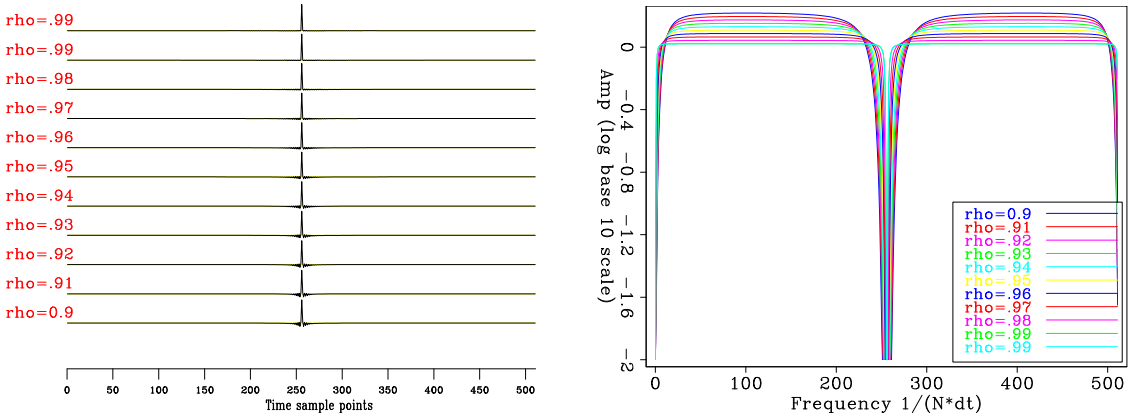

(a) (b)

Figure 7: The test results with large ρ values: (a) in the time domain; (b) in the frequency domain. [**ER**]

However, for our goal (to use the approximate inverse Ricker wavelet as an initial guess for bidirectional deconvolution), we do not need such large ρ values. With large ρ values, the filter will be long and can easily to lead to an unstable result in our deconvolution scheme.

We now have an approximate inverse of the Ricker wavelet separated into two symmetric parts. This matches our requirements for initial guesses for filters f_a and f_b^r. In the next section we will test the approximation using synthetic and field data.

EXAMPLES

Synthetic data example

First we test our initial guess on synthetic data. Because we hope to improve the deconvolution of data with a Ricker-like wavelet, we will test the synthetic data with a Ricker wavelet. We use a 2D reflectivity model to generate our synthetic data. Figure 8(a) shows the model we used, and Figure 1(a) shows our approximate Ricker wavelet (fourth-order) that we used to generate our data. The final synthetic data is shown in Figure 9(a). The wavelet we used is causal, hence we have some time lag in our synthetic data then the spiky model. We use the same deconvolution filter for all traces in our synthetic data example. Figures 10(a) and 10(b) are the result of bidirectional deconvolution using a spike as initial filters for f_a and f_b^r. Figures 11(a) and 11(b) are the result of deconvolution using our approximate inverse Ricker wavelet with ρ=0.7. We see both of the initial guesses (the simple spike and our inverse Ricker wavelet) did a reasonably good job if we see the global view. If we examine the result carefully, we find that the result with the inverse Ricker wavelets as initial guesses has less ghosting, especially in the vicinity of 1.0 s to 1.2 s and 3 km to 5.4 km. This may be more obvious if we see the magnified views of the results. We can also compare them to the magnified views of the synthetic data (Figure 9(b)) and the model (Figure 8(b)), and we find both of bidirectional deconvolution results improve the resolution of events. Figures 12(a) and 12(b) are magnified wiggle plots in the same time window but for just a single trace in the vicinity of 4000 m of CMP_x, from which we can see the the result with inverse Ricker initial guess has less ghosting in wiggle. Although there is improvement, it is not very significant for our synthetic case.

Field data example

We also test our initial guess on a marine common-offset 2D data set. We use the same deconvolution filter for all traces in our field data example as well. Figure 13 shows the 2D input data set. Figure 14 shows the bidirectional deconvolution result with a simple spike as the initial guesses and Figure 15 shows the bidirectional convolution with our inverse Ricker wavelet as the initial guesses, using ρ=0.8.

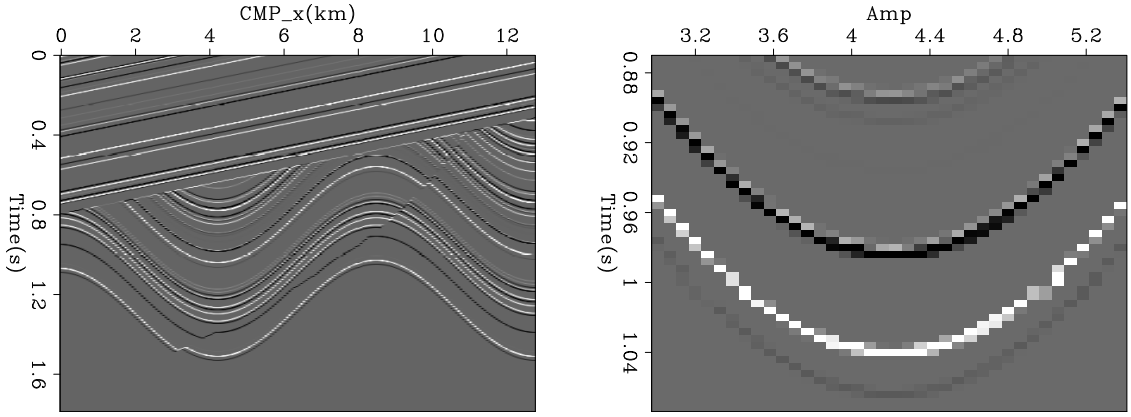

(a) (b)

Figure 8: 2D reflection model we used to to generate our synthetic data: (a) the global view; (b) the magnified view in the time window from .872 s to 1.072 s and in CMP_x range from 3 km to 5.4 km. [**ER**]

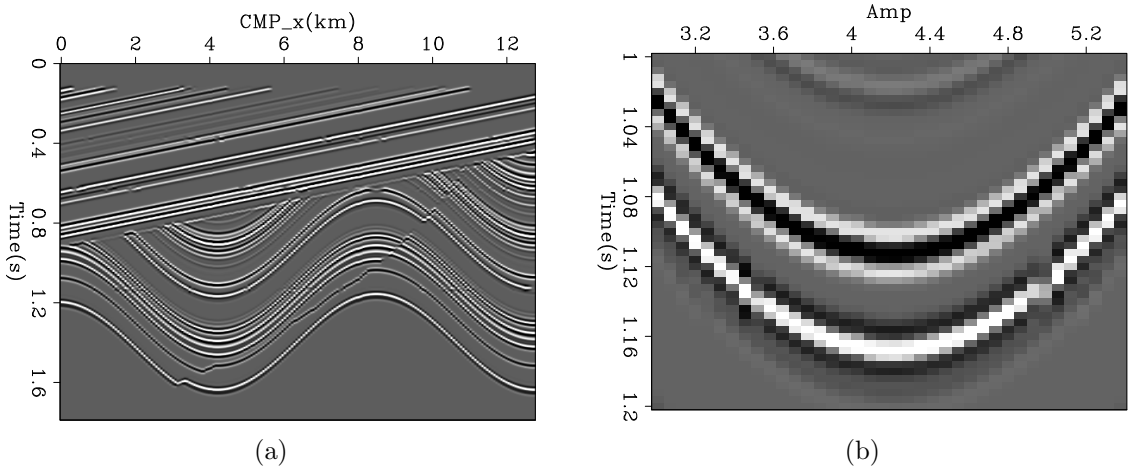

(a) (b)

Figure 9: The synthetic data we used for our test: (a) the global view; (b) the magnified view in the time window from 1 s to 1.2 s and in CMP_x range 3 km to 5.4 km. [**ER**]

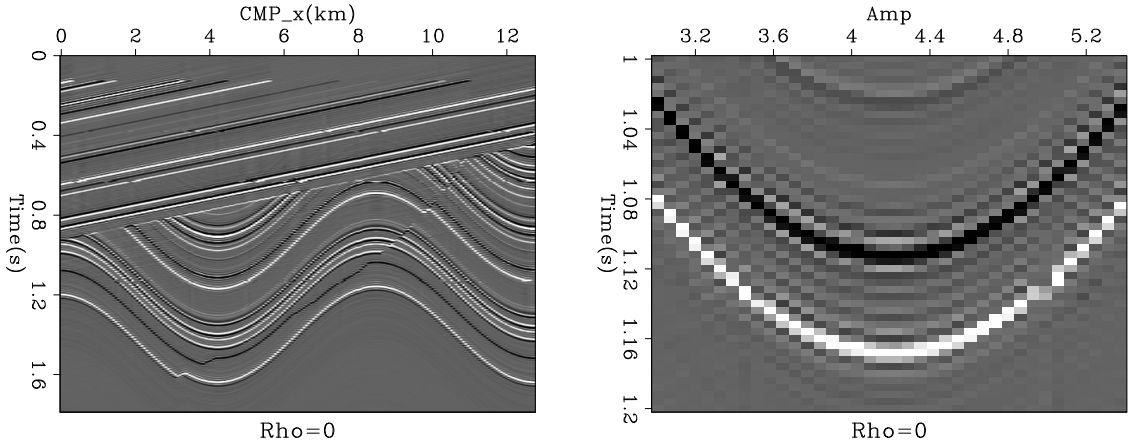

(a) (b)

Figure 10: The result of bidirectional deconvolution using a spike as initial filters f_a and f_b^r on synthetic data: (a) the global view; (b) the magnified view in the time window from 1 s to 1.2 s and in CMP_x range 3 km to 5.4 km. [**ER**]

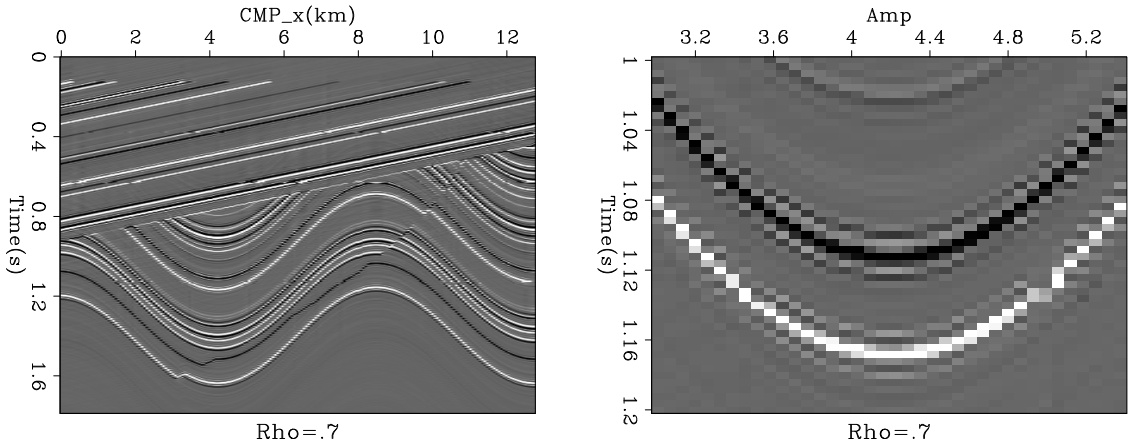

(a) (b)

Figure 11: The result of bidirectional deconvolution using our approximate inverse Ricker wavelet with ρ=0.7 on synthetic data: (a) the global view; (b) the magnified view in the time window from 1 s to 1.2 s and in CMP_x range 3 km to 5.4 km. [**ER**]

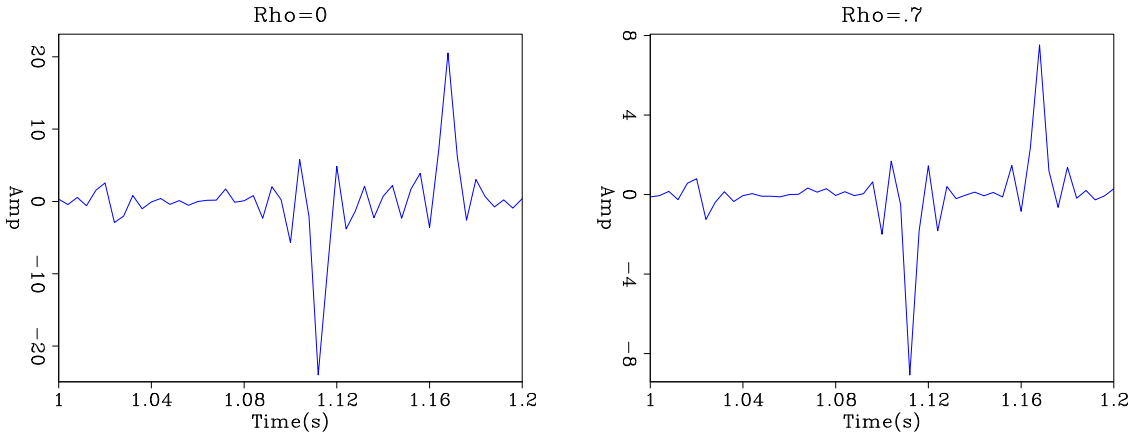

(a) (b)

Figure 12: The magnified wiggle plot of the bidirectional deconvolution results at cmp=4.3 km in the time window from 1 s to 1.2 s: (a) with a spike as the initial guess; (b) with an inverse Ricker wavelet as the initial guess. [**ER**]

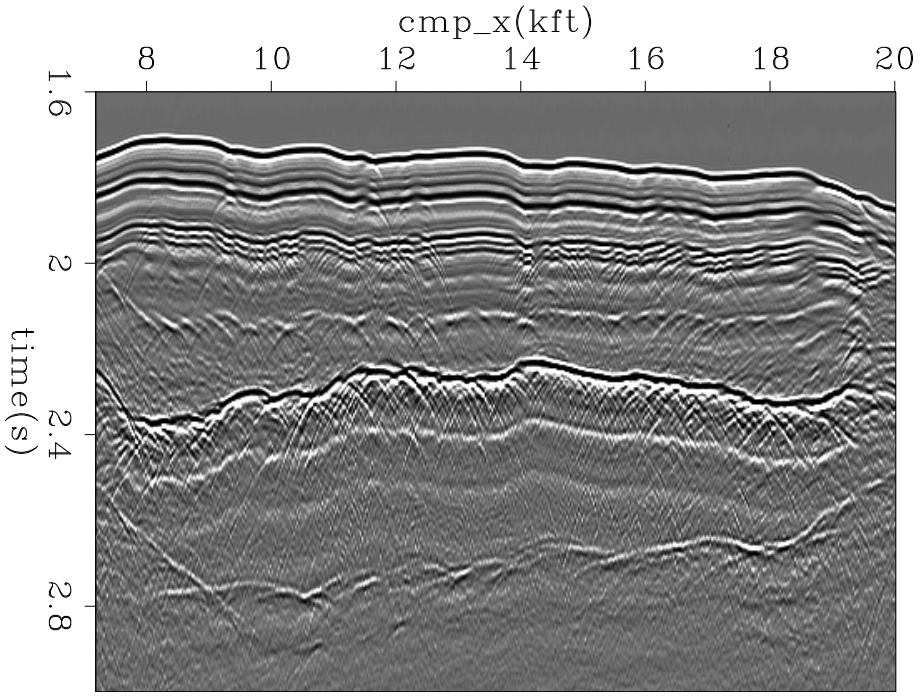

Figure 13: A marine common-offset 2D data set we used for our test. [**ER**]

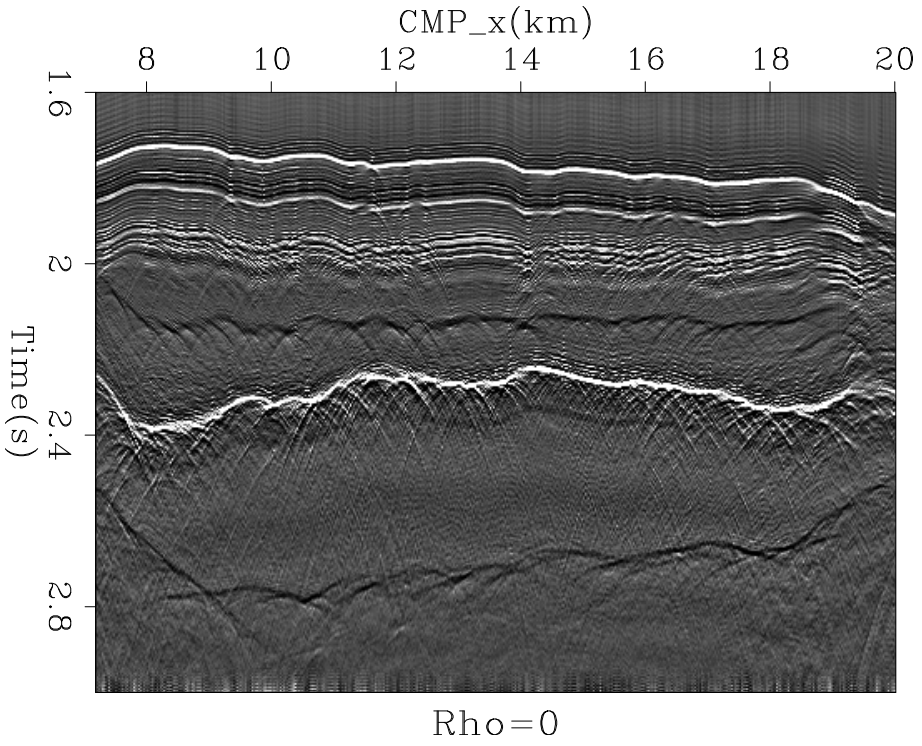

Figure 14: The result of deconvolution using a spike as initial filters f_a and f_b^r on field data. [**ER**]

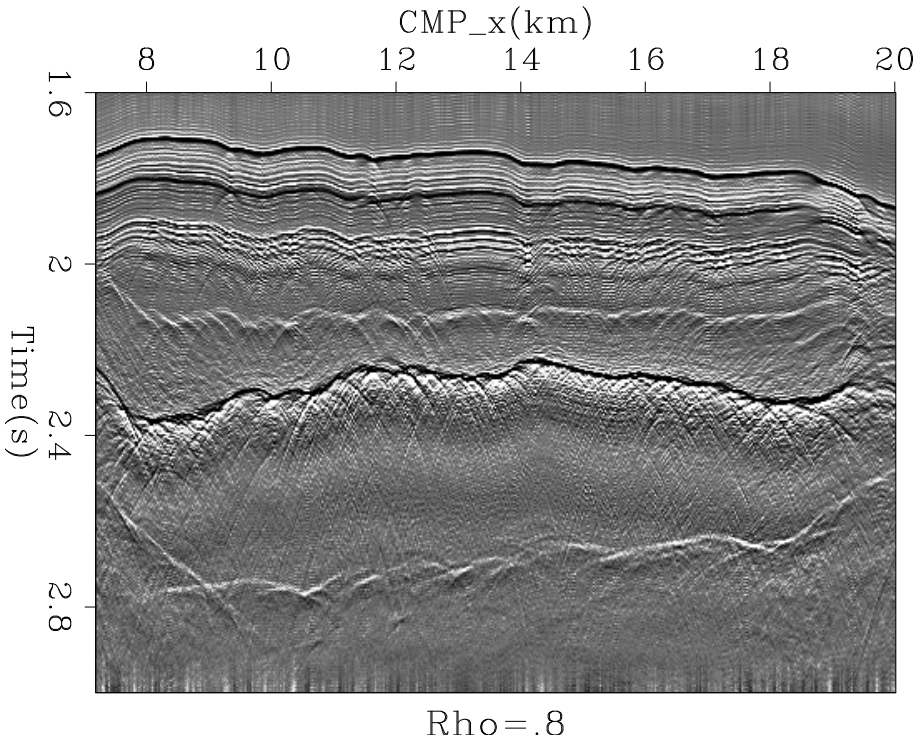

Figure 15: The result of deconvolution using our approximate inverse Ricker wavelet with ρ=0.8 on field data. [**ER**]

It is obvious that the result of using the inverse Ricker wavelet as an initial guess is much better. For example, the ghost events before the first reflection are much suppressed, and the upper boundary of the salt body, which is the event from about 2.2 s to 2.4 s, is condensed. There appears to be a polarity change plus a time shift in our two bidirectional deconvolution output results with different initial guesses. This is not an error. Given the wavelets estimated from deconvolution process, it is a reasonable result.

Figures 16(a) and 16(b) are the wavelets estimated by a simple spike initial guess and our inverse Ricker wavelet initial guess with ρ=0.8. On these wavelet, we can clearly see the airgun bubbles. And the time interval between bubbles are corelate the data shown in 13 very well. The wavelets are causal-like, or in other words, we do not have too much energy in the negative time before the first major impulse. These two evidence indicate that we estimate the wavelet of our field data correctly.However, we still have some problem here. We must mention that we tried to enlarge the filter length to get a longer estimated wavelet by the same scheme, but we got a noisy result. It seems we have some instability here, but we do not know the reason of this now. We are researching this and will explain the reason in furtrue report after we figure it out.

The two wavelets in Figures 16(a) and 16(b) look very similar, but have opposite polarity and a different origin in the time axis. The flipped polarity is caused by the origin shift. Since we have the same input data and wavelet for deconvolution, even with different initial guesses, we should get the same (or at least similar) estimated wavelet and deconvolution filter after the process. Bidirectional deconvolution forces the polarity of both the estimated wavelet and the deconvolution filter to be positive at the origin of the time axis. So if the origin of the estimated wavelet has been shifted from positive to negative, the polarity will be flipped. This estimated wavelet origin shift will cause the output of the deconvolution result to shift on the time axis as well.

CONCLUSIONS

We tested a numerical inversion of the Ricker wavelet as an initial guess for a bidirectional deconvolution scheme. This Ricker wavelet inversion has two symmetric parts, which makes it suitable to be the initial guess. We tested our inversion of the Ricker wavelet on a field data example, and the the inversion of the Ricker wavelet initial guess did improve the bidirectional deconvolution result (with a suitable ρ parameter). We found there is some instability in our scheme if we use different filter length for our deconvolution filter and do not have a explanation of it. We will continue researching on this.

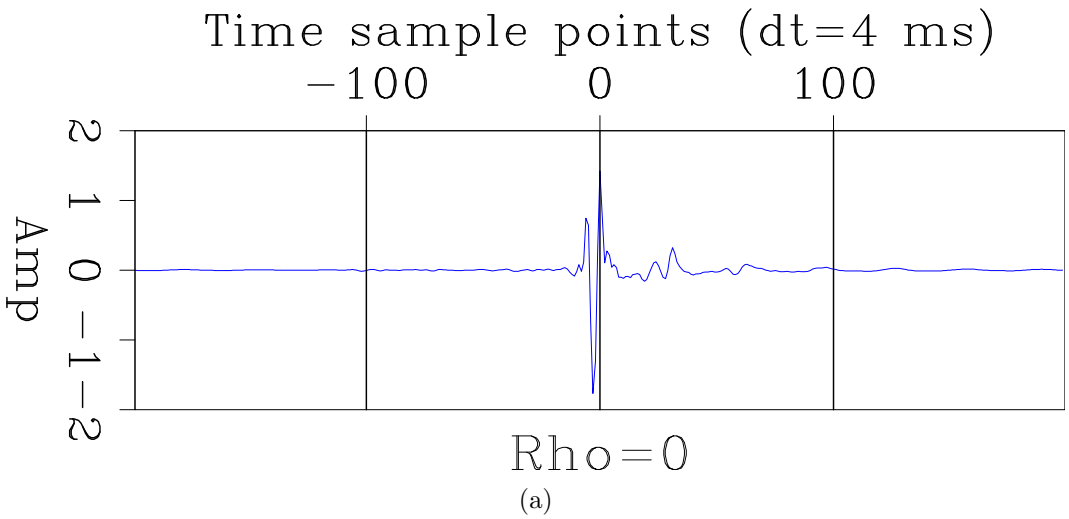

(a)

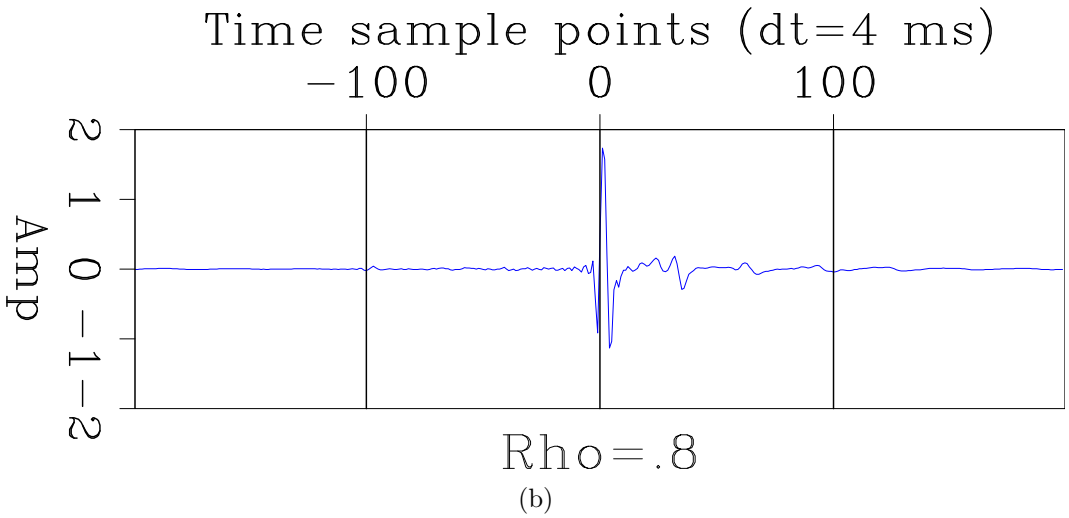

(b)

Figure 16: Estimated wavelet from bidirectional deconvolution on field data: (a) using a spike as initial filters f_a and f_b^r; (b) using our approximate inverse Ricker wavelet with ρ=0.8. [**ER**]

FUTURE WORK

Preconditioning is a well-established technique in linear problems to hasten convergence by utilizing prior information. In non-linear problems such as this, preconditioning may be essential to guide the descent along sensible pathways thus avoiding potential local minima. By adding prior information in the problem, the preconditioning can not only accelerate the convergence but also has the ability to stabilize the result. Because we are facing a unstable problem in our deconvolution implementation, it is our plan to add a preconditioning in the bidirectional deconvolution method for next step. We hope it will help us to increase both the stability and convergence speed of bidirectional deconvolution method.

ACKNOWLEDGMENTS

We would like to thank Yang Zhang, Antoine Guitton, Shuki Ronen, Mandy Wong and Elita Li for helpful discussion of our research.

REFERENCES

Shen, Y., Q. Fu, and J. Claerbout, 2011, A new algorithm for bidirectional deconvolution: SEP-Report, **143**, 271–282.

Zhang, Y. and J. Claerbout, 2010, A new bidirectional deconvolution method that overcomes the minimum phase assumption: SEP-Report, **142**, 93–104.